Intermediate field-induced phase of the honeycomb magnet BaCo$_2$(AsO$_4$)$_2$

Prashanta K. Mukharjee [1,*] Bin Shen [1] Sebastian Erdmann [1] Anton Jesche [1] Julian Kaiser,[1] Priya R. Baral [2]
Oksana Zaharko,[2] Philipp Gegenwart [1,†] and Alexander A. Tsirlin [3,‡]

[1]*Experimental Physics VI, Center for Electronic Correlations and Magnetism, Institute of Physics,*
University of Augsburg, 86159 Augsburg, Germany
[2]*Laboratory for Neutron Scattering and Imaging (LNS), Paul Scherrer Institute (PSI), CH-5232 Villigen, Switzerland*
[3]*Felix Bloch Institute for Solid-State Physics, University of Leipzig, 04103 Leipzig, Germany*

We use magnetometry, calorimetry, and high-resolution capacitive dilatometry, as well as single-crystal neutron diffraction to explore the temperature-field phase diagram of the anisotropic honeycomb magnet BaCo$_2$(AsO$_4$)$_2$. Our data reveal four distinct ordered states observed for in-plane magnetic fields. Of particular interest is the narrow region between 0.51 and 0.54 T that separates the up-up-down order from the fully polarized state and coincides with the field range where signatures of the spin-liquid behavior have been reported. We show that magnetic Bragg peaks persist in this intermediate phase, thus ruling out its spin-liquid nature. However, the simultaneous nonmonotonic evolution of nuclear Bragg peaks suggests the involvement of the lattice, witnessed also in other regions of the phase diagram where large changes in the sample length are observed upon entering the magnetically ordered states. Our data highlight the importance of lattice effects in BaCo$_2$(AsO$_4$)$_2$.

Introduction. A quantum spin liquid (QSL) is an exotic state of matter in which strong quantum fluctuations prevent magnetic long-range order (LRO) down to very low temperatures [1]. The exactly solvable $S = \frac{1}{2}$ honeycomb Kitaev model possessing bond-dependent nearest-neighbor Ising-type interactions offers a promising venue for stabilizing the QSL ground state with the excitation spectrum described by emergent Majorana fermions and gauge fluxes [2]. Experimental realization of this model has been of significant interest. The d^5 (Ir^{4+}, Ru^{3+}) [3] and, more recently, d^7 (Co^{2+}) [4] transition-metal ions were proposed as suitable building blocks of the Kitaev magnets.

The majority of Ir-, Ru-, and Co-based honeycomb materials show long-range order in zero magnetic field [5,6]. However, it was conjectured that they may lie in the vicinity of the QSL phase, and an external field can be used to suppress long-range order, thus giving way to the spin liquid. Indeed, magnetic field applied along a suitable direction leads to a rapid suppression of the ordered phase in α-RuCl$_3$ and β-Li$_2$IrO$_3$ above the critical fields of $B_c \simeq 7$ T and 2.8 T, respectively [7–9]. The behavior of α-RuCl$_3$ above B_c remains vividly debated. Whereas quantized thermal Hall effect [10–12], oscillations in thermal conductivity [13–15], and a distinct excitation continuum [16,17] observed in this field range might be vestiges of the spin-liquid behavior, no distinct phase associated with this putative spin liquid could be identified [18–21].

Here, we focus on the Co-based honeycomb magnet, BaCo$_2$(AsO$_4$)$_2$ (BCAO), recently proposed as a Kitaev candidate [22] with several intriguing analogies to α-RuCl$_3$. The two materials show quite different sequences of the magnetically ordered states, double-zigzag-like and field-induced up-up-down (*uud*) orders in BCAO [23–25] versus different types of zigzag order in α-RuCl$_3$ [26]. Moreover, a detailed study of spin dynamics [27], along with *ab initio* calculations [28], suggested that an easy-plane J_1-J_3 Hamiltonian is more suitable for BCAO than an extended Kitaev model commonly accepted for α-RuCl$_3$ [5]. On the other hand, both materials show several apparent similarities too. They can be polarized by moderate in-plane fields and demonstrate an unusual behavior right above B_c. An excitation continuum in the paramagnetic state [29] and a small linear contribution to the thermal conductivity near B_c [30], which is often associated with spinon excitations, are reminiscent of the spin-liquid physics with the possible field-induced spin-liquid phase.

In the following, we scrutinize the behavior of BCAO in applied magnetic fields. Using several thermodynamic probes, we map out the temperature-field phase diagram of this material and uncover the previously overlooked intermediate phase that appears near B_c and separates the *uud* order from the fully polarized state. This intermediate phase coincides with the field range where linear-in-temperature thermal conductivity has been reported. However, it does not show characteristic signatures of a spin liquid, namely, the absence of the long-range magnetic order, because the magnetic Bragg peak persists in this phase. Our results rule out the formation of the field-induced spin-liquid phase in BCAO and further highlight the importance of spin-lattice coupling in this material, as evidenced by large changes in the sample length across field-induced phase transitions.

———————
*Contact author: pkmukharjee92@gmail.com
†Contact author: philipp.gegenwart@physik.uni-augsburg.de
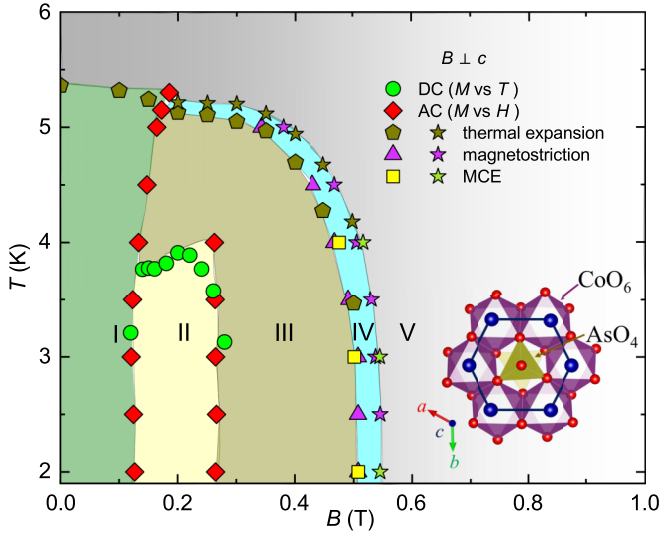‡Contact author: altsirlin@gmail.com

FIG. 1. Magnetic field-temperature (H-T) phase diagram of $BaCo_2(AsO_4)_2$ for $B \perp c$ constructed from magnetization $M(T, B)$, dilatometry $L(T, B)$, and MCE measurements. Phase diagrams for different in-plane field directions are shown in Fig. S12 [31]. Inset: A honeycomb motif containing CoO_6 octahedra and AsO_4 tetrahedra at the center. The individual Co-honeycomb layers are stacked along the c axis with Ba atoms separating them.

Methods. Dark-pink-colored single crystals of BCAO were synthesized by the flux method [31]. The high quality of these crystals was confirmed by an extensive mapping with Laue diffraction and by neutron diffraction (see Fig. S1). Temperature- and field-dependent magnetization was measured using a commercial superconducting quantum interference device (SQUID) magnetometer (MPMS3, Quantum Design), with orientation-dependent magnetization data collected using the sample rotation stage of MPMS3. Specific heat was measured using a standard relaxation technique in a Quantum Design physical properties measurement system (QD PPMS). The magnetic Grüneisen parameter (Γ_m), which equals the adiabatic magnetocaloric effect (MCE), was determined by the alternating-field method [32]. Thermal expansion was measured with the aid of a compact ultrahigh-resolution capacitive dilatometer in the QD PPMS [33]. The length change as a function of temperature or field was recorded using a capacitance bridge (Andeen Haggerling 2550A). Neutron diffraction data from a single crystal were collected on the ZEBRA diffractometer at SINQ, Paul Scherrer Institute.

Phase diagram. A previous report revealed an almost isotropic behavior of BCAO within the honeycomb plane [27], in contrast to α-RuCl$_3$ that showed different phase boundaries for two nonequivalent in-plane field directions, b and b^* [21,26]. Our data for BCAO confirm this isotropic in-plane behavior. Therefore, in Fig. 1 we merged the data points obtained for different field directions, whereas individual phase diagrams for $B\|b$ and $B\|b^*$ can be found in the Supplemental Material [31] (Fig. S12). In magnetometry, we determine temperature and field values of the transitions from the peak positions of the respective derivatives. In dilatometry, we consider the peak positions of linear thermal expansion coefficient (α) and magnetostriction (λ), while in the MCE (Γ_m) data, we

identify the transitions from the positions of the minima and zero crossings [21].

Two magnetically ordered states of BCAO, the incommensurate double-zigzag order and commensurate *uud* order [23–25], are labeled as phases I and III in our phase diagram, respectively. Phase V is the fully polarized state. Additionally, we uncover phases II and IV that separate I from III and III from V, respectively. Phase IV is of particular interest, as it coincides with the field range of the putative spin liquid in $BaCo_2(AsO_4)_2$ [30].

Temperature-dependent dc magnetization of BCAO (Fig. S2) shows an abrupt drop at T_N followed by a broad maximum that appears between 0.12 and 0.26 T, the field range that we identify as phase II. The boundaries of this phase are most clearly visible in the ac susceptibility that shows two consecutive peaks as a function of field [Fig. 2(a)]. The lower boundary of phase II is characterized by the abrupt increase in $M(B)$, suggesting that the transformation from the antiferromagnetic double zigzag into the partially polarized *uud* state starts upon entering phase II. This transformation is first order in nature, as witnessed by the large field hysteresis (Fig. S4). The anomalies associated with phase II disappear around 4 K, whereas phases I and III survive up to 5.2–5.3 K.

The transition between I and III involves a flip of ferromagnetic zigazag spin chains from the ↑↑↓↓↑↑↓↓ into the ↑↑↓↑↑↓ configuration, which is essentially the creation and shift of domain walls. It is plausible that such a shift requires thermal energy and at lower temperatures involves an intermediate region, which we identify as phase II. This phenomenology may be similar to the isostructural $BaCo_2(PO_4)_2$ where the magnetization curve shows distinct steps that correspond to discrete shifts of the domain walls, albeit at temperatures below 1 K only [34].

We now turn to thermal expansion (TE) and magnetostriction (MS) where all phase transitions are clearly visible thanks to the large lattice effects involved. BCAO shrinks along c upon entering phase I and expands along c upon entering phase III, but the most interesting behavior is seen in temperature-dependent thermal expansion measured above 0.2 T where the sample length changes nonmonotonically indicating two consecutive phase transitions, first with the decrease and then with the increase in c upon cooling [Fig. 3(a)]. A similar behavior is seen in the field-dependent sample length that changes nonmonotonically on going from phase III into phase V [Fig. 3(c)]. The two transitions can be tracked using the minima and maxima in linear thermal expansion coefficient $\alpha = (1/L_0)(d \Delta L/dT)$ and magnetostriction $\lambda = (1/L_0)(d \Delta L/dB)$ [Figs. 3(b) and 3(d)], resulting in the distinct region of phase IV that envelops phase III and separates it from phase V. This phase IV is remarkably different from phase II because it extends in temperature all the way up to 5.3 K where BCAO enters its paramagnetic state. Moreover, the transitions associated with phase IV should be second order or weakly first order in nature, as they do not show any significant hysteresis.

Intermediate phase. Phase IV is most clearly seen in the thermal expansion and magnetostriction data. It is further evidenced by the differential susceptibility dM/dB where the double peak at 0.50–0.54 T demonstrates that phase III transforms into phase V via the intermediate phase IV
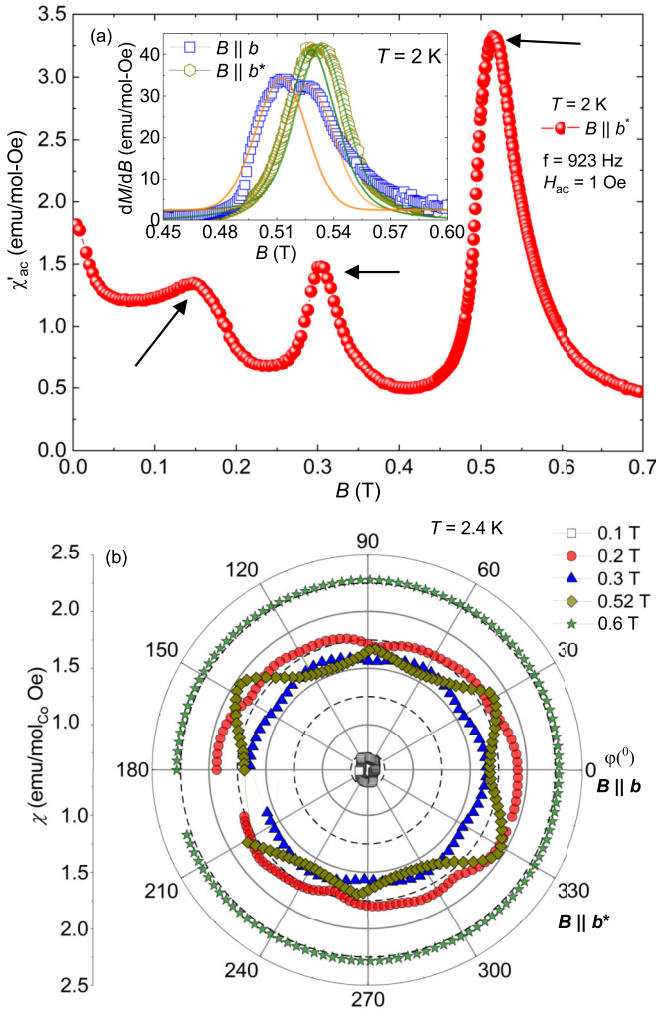
FIG. 2. (a) Magnetic field dependence of the ac susceptibility χ'_{ac} at 2 K for $B||b^*$. The arrow marks indicate the position of the respective phase boundaries. The inset shows the differential susceptibility dM/dB obtained from dc-magnetization measurements. The double peak in dM/dB confirms the formation of phase IV. The solid lines are visual guides, illustrating the separation of the two peaks. (b) Angle-dependent magnetic susceptibility measured at $T = 2.4$ K for different magnetic fields while rotating the crystal in the ab plane. Note the change in the positions of the minima and maxima between 0.3 T (phase III) and 0.52 T (phase IV).
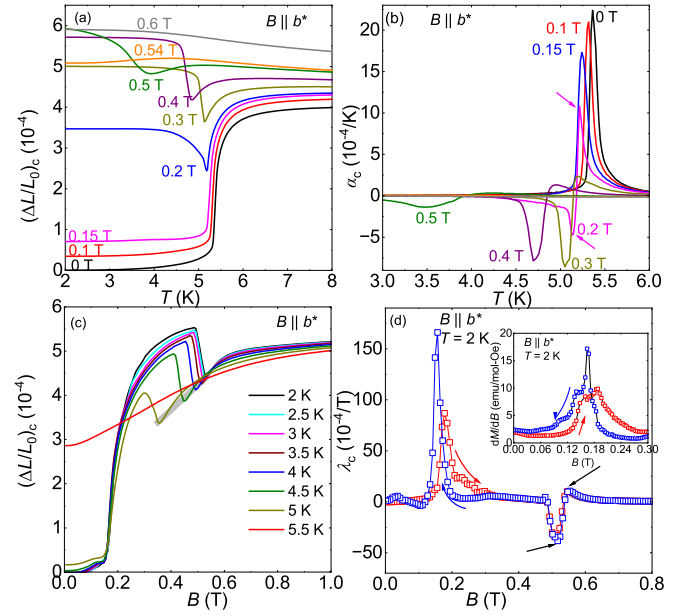

FIG. 3. Thermal expansion and magnetostriction plots of BCAO. (a) Normalized relative length changes vs temperature measured while warming at various fields. The curves are shifted vertically for clarity. (b) Plot of the linear TE coefficient (α) in different fields. For $B = 0$ T, in phase I, α shows a positive peak. As we move into phase II, α bifurcates into two peaks with opposite sign as indicated by the arrows. (c) Normalized relative length changes vs magnetic field measured while sweeping magnetic field up at several temperatures above and below T_N. The light gray line is a guide to eye showing the systematic shift of minimum around B_c. (d) Plot of linear MS coefficient λ vs B at $T = 2$ K. Two prominent peaks are indicated by arrows around B_c. The transition around 0.15 T exhibits significant hysteresis, consistent with the field-dependent differential susceptibility (inset), reflecting its first-order nature.

[Fig. 2(a), inset]. The MCE measurement Γ_m displays the minimum and zero crossing at the III-IV and IV-V boundaries, respectively (see Fig. S10). Finally, angle-dependent susceptibility reveals a clear change from the sixfold symmetric response at 0.3 T, as expected for the *uud* state (phase III) in the $R\bar{3}$ crystal structure, to a weakly deformed hexagon at 0.52 T within phase IV [Fig. 2(b)]. This hexagon is turned by 30°, such that the minima and maxima of the susceptibility are swapped, indicating a qualitative change in the in-plane magnetic anisotropy between phases III and IV.

We further probed phase IV using neutron diffraction. In phase III, we observed the magnetic Bragg peak at $\mathbf{q} = (\frac{1}{3}, 0, -\frac{4}{3})$ in agreement with the previous studies [24,27]. This peak is also observed between 0.50 and 0.54 T, in the field range of phase IV, but gradually loses

its intensity and vanishes when the fully polarized state is reached (see Fig. 4). In order to probe whether this evolution of the magnetic Bragg peak could merely indicate a gradual reduction in the ordered magnetic moment, we further tracked the nuclear Bragg peaks across the same field range. A direct transformation between phases III and V with the phase coexistence between 0.50 and 0.54 T should lead to the gradual increase in the intensity of the nuclear Bragg peaks through the shift of the magnetic intensity from $\mathbf{q} = (\frac{1}{3}, 0, -\frac{4}{3})$ to $\mathbf{q} = \mathbf{0}$ as magnetization increases. However, the $\mathbf{q} = \mathbf{0}$ intensities change nonmonotonically, as shown in Fig. 4 for a representative nuclear Bragg peak. We thus conclude that a distinct phase IV appears between 0.50 and 0.54 T, in agreement with thermodynamic measurements where the double transition is observed in differential susceptibility, thermal expansion, and magnetostriction.

Pressure dependence of the transitions. Magnetic transitions in BCAO are accompanied by remarkably large lattice effects. For example, the zero-field transition between the paramagnetic phase and phase I corresponds to the relative length change of 4×10^{-4}, about four times larger than in α-RuCl$_3$ [20]. It indicates the unusually strong spin-lattice coupling in BCAO.
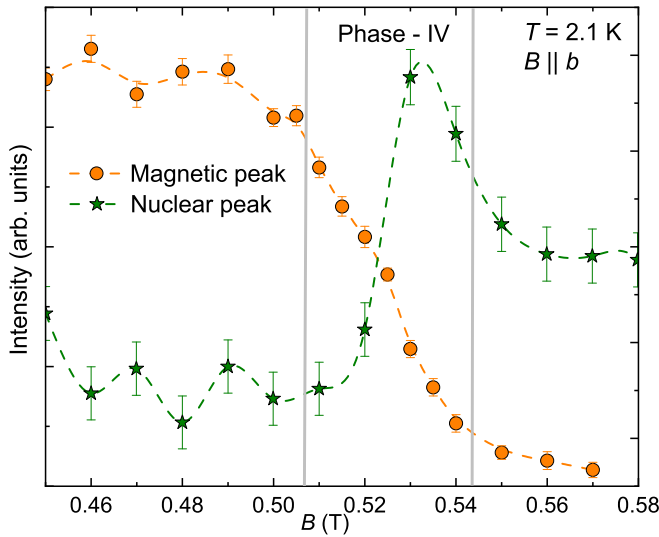
FIG. 4. Magnetic field dependence of the magnetic Bragg peak at $\mathbf{q} = (1/3, 0, -4/3)$ and nuclear Bragg peak at $\mathbf{q} = (3, 0, 0)$ across phase IV for $B \parallel b$.

To explore manifestations of this spin-lattice coupling, we analyze the initial pressure dependence of the magnetic transitions using the peaks in α and λ. According to Maxwell's relation, $\lambda V = -(dM/dp)_{T,B}$, where V is the volume and M is the magnetization. Whereas we do not measure volume magnetostriction in our experiments, the qualitative behavior given by the positive ($\lambda_c > 0$) and negative peaks ($\lambda_c < 0$) in linear magnetostriction suggests that external pressure should decrease the magnetization in phase I and increase it in phase III. The former trend is indeed confirmed by our isothermal magnetization measurements performed under hydrostatic pressure [Fig. S11(c)].

The pressure dependence of the transition temperature, dT_N/dp, is given by the Clausius-Clapeyron and Ehrenfest relations for the first- and second-order transitions, respectively. From the maxima and minima in α_c, we expect T_N to increase with pressure in phase I and decrease with pressure in phase III. These trends are again consistent with the direct magnetization measurements under hydrostatic pressure using both our data [31] and the earlier report [35]. The phase diagram of BCAO drastically changes under pressure because the $\frac{1}{3}$ plateau is no longer seen at 1.6 GPa [31]. It means that phase III gives way to some other phase that allows a gradual increase in the magnetization, in contrast to the *uud* order that keeps the magnetization fixed at $\frac{1}{3}$ of the saturated value. One interesting possibility is that phase III may be fully replaced by phase IV under pressure.

Discussion. Our data rule out the spin-liquid behavior of BCAO in the vicinity of B_c. Although we observe a distinct presaturation phase, the persistence of the magnetic Bragg peak indicates the presence of long-range order all the way up to 0.54 T where the fully polarized state sets in. This absence of the field-induced spin-liquid phase undermines the consideration of BCAO as a candidate Kitaev material.

At first glance, phase IV of BCAO could be paralleled to the so-called zz2 phase reported in α-RuCl$_3$ [21,26] above 6 T. This phase is magnetically ordered and characterized by the swapped maxima and minima of the angle-dependent

susceptibility [26], similar to phase IV of BCAO [Fig. 2(b)]. The zz2 phase of α-RuCl$_3$ further shows the six-layer periodicity of the magnetic order, in contrast to the three-layer periodicity in lower fields. However, we did not detect any significant change in the interlayer component of the magnetic order of BCAO within phase IV. Therefore, the direct analogy to α-RuCl$_3$, even on the level of its magnetically ordered phases, seems unlikely.

From the theoretical perspective, possible phases of J_1-J_3 frustrated honeycomb ferromagnets have been studied in detail [36–38]. Whereas spin liquid could be stable in a very narrow range of parameters [37], the observation of the magnetic Bragg peak up to the full saturation at 0.54 T speaks against the formation of this spin-liquid phase in BCAO. The V-type order proposed as one of the possible field-induced phases [39] is also unlikely, because it should be characterized by a different propagation vector compared to the *uud* state. We are thus led to conclude that the existing theoretical framework does not offer a microscopic explanation for the formation of phase IV. It seems likely that the appearance of this phase is influenced by the spin-lattice coupling that has not been considered in Kitaev materials to date, although it is known to stabilize nontrivial field-induced phases in pyrochlore [40,41] and triangular [42] magnets. Experimental signatures of the spin-lattice coupling in BCAO include (i) large lattice changes upon the magnetic transitions, and (ii) loss of the sixfold symmetry within phase IV, in contrast to phase III characterized by the sixfold-symmetric magnetic susceptibility.

The intermediate phase observed in our work does not cover the full field range where indications of the spin liquid have been reported. Indeed, the linear-in-temperature contribution to the thermal conductivity extends up to 0.6 T [30], well into the fully polarized state. However, the onset of this unusual behavior at 0.50 T is clearly correlated with the formation of phase IV and not with reaching the fully polarized state around 0.55 T, so the presence of this intermediate phase must be taken into consideration when the microscopic scenario of the spin-liquid-like behavior of BCAO is looked for.

Conclusions. Our comprehensive study of the anisotropic honeycomb magnet BaCo$_2$(AsO$_4$)$_2$ rules out the existence of a distinct spin-liquid phase near B_c and reveals instead a narrow intermediate phase with persistent magnetic order. Large lattice changes accompanying all magnetic transitions, as well as the loss of the sixfold symmetry within the intermediate phase, indicate the importance of spin-lattice coupling in this material. Whereas BaCo$_2$(AsO$_4$)$_2$ does not show any clear-cut manifestations of the Kitaev physics, it may serve as an interesting case of a frustrated honeycomb ferromagnet where competing magnetic phases are controlled by lattice effects.

[1] C. Broholm, R. J. Cava, S. A. Kivelson, D. G. Nocera, M. R. Norman, and T. Senthil, Quantum spin liquids, Science **367**, eaay0668 (2020).

[2] A. Kitaev, Anyons in an exactly solved model and beyond, Ann. Phys. **321**, 2 (2006).

[3] G. Jackeli and G. Khaliullin, Mott insulators in the strong spin-orbit coupling limit: From Heisenberg to a quantum compass and Kitaev models, Phys. Rev. Lett. **102**, 017205 (2009).

[4] H. Liu and G. Khaliullin, Pseudospin exchange interactions in d^7 cobalt compounds: Possible realization of the Kitaev model, Phys. Rev. B **97**, 014407 (2018).

[5] S. M. Winter, A. A. Tsirlin, M. Daghofer, J. van den Brink, Y. Singh, P. Gegenwart, and R. Valentí, Models and materials for generalized Kitaev magnetism, J. Phys.: Condens. Matter **29**, 493002 (2017).

[6] C. Kim, H.-S. Kim, and J.-G. Park, Spin-orbital entangled state and realization of Kitaev physics in $3d$ cobalt compounds: a progress report, J. Phys.: Condens. Matter **34**, 023001 (2022).

[7] H. Takagi, T. Takayama, G. Jackeli, G. Khaliullin, and S. E. Nagler, Concept and realization of Kitaev quantum spin liquids, Nat. Rev. Phys. **1**, 264 (2019).

[8] A. Ruiz, A. Frano, N. P. Breznay, I. Kimchi, T. Helm, I. Oswald, J. Y. Chan, R. J. Birgeneau, Z. Islam, and J. G. Analytis, Correlated states in β-Li$_2$IrO$_3$ driven by applied magnetic fields, Nat. Commun. **8**, 961 (2017).

[9] M. Majumder, F. Freund, T. Dey, M. Prinz-Zwick, N. Büttgen, Y. Skourski, A. Jesche, A. A. Tsirlin, and P. Gegenwart, Anisotropic temperature-field phase diagram of single crystalline β-Li$_2$IrO$_3$: Magnetization, specific heat, and ^{7}Li NMR study, Phys. Rev. Mater. **3**, 074408 (2019).

[10] T. Yokoi, S. Ma, Y. Kasahara, S. Kasahara, T. Shibauchi, N. Kurita, H. Tanaka, J. Nasu, Y. Motome, C. Hickey, S. Trebst, and Y. Matsuda, Half-integer quantized anomalous thermal Hall effect in the Kitaev material candidate α-RuCl$_3$, Science **373**, 568 (2021).

[11] E. Lefrançois, G. Grissonnanche, J. Baglo, P. Lampen-Kelley, J.-Q. Yan, C. Balz, D. Mandrus, S. E. Nagler, S. Kim, Y.-J. Kim, N. Doiron-Leyraud, and L. Taillefer, Evidence of a phonon Hall effect in the Kitaev spin liquid candidate α-RuCl$_3$, Phys. Rev. X **12**, 021025 (2022).

[12] J. A. N. Bruin, R. R. Claus, Y. Matsumoto, N. Kurita, H. Tanaka, and H. Takagi, Robustness of the thermal Hall effect close to half-quantization in α-RuCl$_3$, Nat. Phys. **18**, 401 (2022).

[13] P. Czajka, T. Gao, M. Hirschberger, P. Lampen-Kelley, A. Banerjee, J. Yan, D. G. Mandrus, S. E. Nagler, and N. P. Ong, Oscillations of the thermal conductivity in the spin-liquid state of α-RuCl$_3$, Nat. Phys. **17**, 915 (2021).

[14] E. Lefrançois, J. Baglo, Q. Barthélemy, S. Kim, Y.-J. Kim, and L. Taillefer, Oscillations in the magnetothermal conductivity of α-RuCl$_3$: Evidence of transition anomalies, Phys. Rev. B **107**, 064408 (2023).

[15] J. A. N. Bruin, R. R. Claus, Y. Matsumoto, J. Nuss, S. Laha, B. V. Lotsch, N. Kurita, H. Tanaka, and H. Takagi, Origin of oscillatory structures in the magnetothermal conductivity of the putative Kitaev magnet α-RuCl$_3$, APL Mater. **10**, 090703 (2022).

[16] A. Banerjee, P. Lampen-Kelley, J. Knolle, C. Balz, A. A. Aczel, B. Winn, Y. Liu, D. Pajerowski, J. Yan, C. A. Bridges, A. T. Savici, B. C. Chakoumakos, M. D. Lumsden, D. A. Tennant, R. Moessner, D. G. Mandrus, and S. E. Nagler, Excitations

[17] A. Sahasrabudhe, M. A. Prosnikov, T. C. Koethe, P. Stein, V. Tsurkan, A. Loidl, M. Grüninger, H. Hedayat, and P. H. M. van Loosdrecht, Chiral excitations and the intermediate-field regime in the Kitaev magnet α-RuCl$_3$, Phy. Rev. Res. **6**, L022005 (2024).

[18] S. Bachus, D. A. S. Kaib, Y. Tokiwa, A. Jesche, V. Tsurkan, A. Loidl, S. M. Winter, A. A. Tsirlin, R. Valentí, and P. Gegenwart, Thermodynamic perspective on field-induced behavior of α-RuCl$_3$, Phys. Rev. Lett. **125**, 097203 (2020).

[19] R. Schönemann, S. Imajo, F. Weickert, J. Yan, D. G. Mandrus, Y. Takano, E. L. Brosha, P. F. S. Rosa, S. E. Nagler, K. Kindo, and M. Jaime, Thermal and magnetoelastic properties of α-RuCl$_3$ in the field-induced low-temperature states, Phys. Rev. B **102**, 214432 (2020).

[20] S. Gass, P. M. Cônsoli, V. Kocsis, L. T. Corredor, P. Lampen-Kelley, D. G. Mandrus, S. E. Nagler, L. Janssen, M. Vojta, B. Büchner, and A. U. B. Wolter, Field-induced transitions in the Kitaev material α-RuCl$_3$ probed by thermal expansion and magnetostriction, Phys. Rev. B **101**, 245158 (2020).

[21] S. Bachus, D. A. S. Kaib, A. Jesche, V. Tsurkan, A. Loidl, S. M. Winter, A. A. Tsirlin, R. Valentí, and P. Gegenwart, Angle-dependent thermodynamics of α-RuCl$_3$, Phys. Rev. B **103**, 054440 (2021).

[22] R. Zhong, T. Gao, N. P. Ong, and R. J. Cava, Weak-field induced nonmagnetic state in a Co-based honeycomb, Sci. Adv. **6**, eaay6953 (2020).

[23] L. Regnault, P. Burlet, and J. Rossat-Mignod, Magnetic ordering in a planar XY model: BaCo$_2$(AsO$_4$)$_2$, Physica B+C **86-88**, 660 (1977).

[24] L. P. Regnault and J. Rossat-Mignod, Effect of a magnetic field on the magnetic ordering of BaCo$_2$(AsO$_4$)$_2$, J. Magn. Magn. Mater. **14**, 194 (1979).

[25] L.-P. Regnault, C. Boullier, and J. Lorenzo, Polarized-neutron investigation of magnetic ordering and spin dynamics in BaCo$_2$(AsO$_4$)$_2$ frustrated honeycomb-lattice magnet, Heliyon **4**, e00507 (2018).

[26] C. Balz, L. Janssen, P. Lampen-Kelley, A. Banerjee, Y. H. Liu, J.-Q. Yan, D. G. Mandrus, M. Vojta, and S. E. Nagler, Field-induced intermediate ordered phase and anisotropic interlayer interactions in α-RuCl$_3$, Phys. Rev. B **103**, 174417 (2021).

[27] T. Halloran, F. Desrochers, E. Z. Zhang, T. Chen, L. E. Chern, Z. Xu, B. Winn, M. Graves-Brook, M. B. Stone, A. I. Kolesnikov, Y. Qiu, R. Zhong, R. Cava, Y. B. Kim, and C. Broholm, Geometrical frustration versus Kitaev interactions in BaCo$_2$(AsO$_4$)$_2$, Proc. Natl. Acad. Sci. USA **120**, e2215509119 (2023).

[28] P. A. Maksimov, A. V. Ushakov, Z. V. Pchelkina, Y. Li, S. M. Winter, and S. V. Streltsov, *Ab initio* guided minimal model for the "Kitaev" material BaCo$_2$(AsO$_4$)$_2$: Importance of direct hopping, third-neighbor exchange, and quantum fluctuations, Phys. Rev. B **106**, 165131 (2022).

[29] X. Zhang, Y. Xu, T. Halloran, R. Zhong, C. Broholm, R. J. Cava, N. Drichko, and N. P. Armitage, A magnetic continuum in the cobalt-based honeycomb magnet BaCo$_2$(AsO$_4$)$_2$, Nat. Mater. **22**, 58 (2023).

[30] C. Tu, D. Dai, X. Zhang, C. Zhao, X. Jin, B. Gao, T. Chen, P. Dai, and S. Li, Evidence for gapless quantum spin liquid in a honeycomb lattice, arXiv:2212.07322.

[31] See Supplemental Material at http://link.aps.org/supplemental/10.1103/PhysRevB.110.L140407 for details of the experimental methods and sample characterization, as well as phase diagrams for different in-plane field directions, which also includes Refs. [44–46].

[32] Y. Tokiwa and P. Gegenwart, High-resolution alternating-field technique to determine the magnetocaloric effect of metals down to very low temperatures, Rev. Sci. Instrum. **82**, 013905 (2011).

[33] R. Küchler, A. Wörl, P. Gegenwart, M. Berben, B. Bryant, and S. Wiedmann, The world's smallest capacitive dilatometer, for high-resolution thermal expansion and magnetostriction in high magnetic fields, Rev. Sci. Instrum. **88**, 083903 (2017).

[34] X. Wang, R. Sharma, P. Becker, L. Bohatý, and T. Lorenz, Single-crystal study of the honeycomb XXZ magnet $BaCo_2(PO_4)_2$ in magnetic fields, Phys. Rev. Mater. **7**, 024402 (2023).

[35] S. Huyan, J. Schmidt, E. Gati, R. Zhong, R. J. Cava, P. C. Canfield, and S. L. Bud'ko, Hydrostatic pressure effect on the Co-based honeycomb magnet $BaCo_2(AsO_4)_2$, Phys. Rev. B **105**, 184431 (2022).

[36] S. Jiang, S. R. White, and A. L. Chernyshev, Quantum phases in the honeycomb-lattice J_1-J_3 ferro-antiferromagnetic model, Phys. Rev. B **108**, L180406 (2023).

[37] A. Bose, M. Routh, S. Voleti, S. K. Saha, M. Kumar, T. Saha-Dasgupta, and A. Paramekanti, Proximate Dirac spin liquid in the honeycomb lattice J_1-J_3 XXZ model: Numerical study and application to cobaltates, Phys. Rev. B **108**, 174422 (2023).

[38] Y. Watanabe, S. Trebst, and C. Hickey, Frustrated ferromagnetism of honeycomb cobaltates: Incommensurate spirals, quantum disordered phases, and out-of-plane Ising order, arXiv:2212.14053.

[39] P. A. Maksimov, Proximity-induced sequence of field transitions in the Kitaev candidate $BaCo_2(AsO_4)_2$, Phys. Rev. B **108**, L180405 (2023).

[40] A. Miyata, H. Suwa, T. Nomura, L. Prodan, V. Felea, Y. Skourski, J. Deisenhofer, H.-A. Krug von Nidda, O. Portugall, S. Zherlitsyn, V. Tsurkan, J. Wosnitza, and A. Loidl, Spin-lattice coupling in a ferrimagnetic spinel: Exotic H-T phase diagram of $MnCr_2S_4$ up to 110 T, Phys. Rev. B **101**, 054432 (2020).

[41] M. Gen, A. Ikeda, K. Aoyama, H. O. Jeschke, Y. Ishii, H. Ishikawa, T. Yajima, Y. Okamoto, X. Zhou, D. Nakamura, S. Takeyama, K. Kindo, Y. H. Matsuda, and Y. Kohama, Signatures of a magnetic superstructure phase induced by ultrahigh magnetic fields in a breathing pyrochlore antiferromagnet, Proc. Natl. Acad. Sci. USA **120**, e2302756120 (2023).

[42] T. Nakajima, N. Terada, S. Mitsuda, and R. Bewley, Spin-driven bond order in a 1/5-magnetization plateau phase in the triangular lattice antiferromagnet $CuFeO_2$, Phys. Rev. B **88**, 134414 (2013).

[43] P. K. Mukharjee, B. Shen, S. Erdmann, A. Jesche, J. Kaiser, P. R. Baral, O. Zaharko, P. Gegenwart, and A. A. Tsirlin, Intermediate field-induced phase of the honeycomb magnet $BaCo_2(AsO_4)_2$ (data set), https://zenodo.org/doi/10.5281/zenodo.10721313.

[44] J. Rodríguez-Carvajal, Recent advances in magnetic structure determination by neutron powder diffraction, Phys. B: Condens. Matter **192**, 55 (1993).

[45] R. D. Johnson, S. C. Williams, A. A. Haghighirad, J. Singleton, V. Zapf, P. Manuel, I. I. Mazin, Y. Li, H. O. Jeschke, R. Valentí, and R. Coldea, Monoclinic crystal structure of α-$RuCl_3$ and the zigzag antiferromagnetic ground state, Phys. Rev. B **92**, 235119 (2015).

[46] J.-Q. Yan, S. Okamoto, Y. Wu, Q. Zheng, H. D. Zhou, H. B. Cao, and M. A. McGuire, Magnetic order in single crystals of $Na_3Co_2SbO_6$ with a honeycomb arrangement of $3d^7Co^{2+}$ ions, Phys. Rev. Mater. **3**, 074405 (2019).